Spin-Density Wave in Ultrathin Fe Films on Cu(100)

D. Qian and X. F. Jin*
Surface Physics Laboratory, Fudan University, Shanghai 200433, China
and Max-Planck-Institut für Mikrostrukturphysik, Weinberg 2, D-06120 Halle/Saale, Germany

J. Barthel, M. Klaua, and J. Kirschner
Max-Planck-Institut für Mikrostrukturphysik, Weinberg 2, D-06120 Halle/Saale, Germany
(Received 12 April 2001; published 12 November 2001)

For Fe films epitaxially grown on Cu(100) at 300 K, the total magnetic moment as a function of film thickness and its temperature dependence have been investigated *in situ* with a multitechnique approach. The results exclude the collinear type-1 antiferromagnetic configuration as the magnetic structure for face-centered-cubic Fe films on Cu(100). It is proposed that a spin-density-wave state is responsible for the magnetic structure.

DOI: 10.1103/PhysRevLett.87.227204 PACS numbers: 75.30.Fv

Among the magnetic $3d$ transition metals in their elemental form, Cr and Mn have the strong tendency to be antiferromagnetic (AFM) at low temperature, while on the other hand Co and Ni are always found to be ferromagnetic (FM) at low temperature. As an element located between the two extremes, Fe exhibits a rich variety of magnetic phases. While body-centered-cubic (bcc) Fe is the prototype ferromagnet, face-centered-cubic (fcc) Fe is predicted to be nonmagnetic, antiferromagnetic, ferromagnetic, or spin-density-wave, depending on the lattice constant [1–7]. Experimentally, it is known that bulk fcc Fe exists only at temperatures above 910 °C. However, the low temperature fcc Fe phase can be stabilized as small particles ($d \sim 50$ nm) in a Cu matrix, and its magnetic structure has been determined to be an antiferromagnetic incommensurate spin-density wave (SDW) [8,9].

In fact, the low temperature fcc Fe phase can also be stabilized by epitaxial growth on a Cu(100) substrate. Presumably it is one of the most challenging and controversial magnetic thin-film systems to date because of its structural and magnetic instability [10]. With an extensive amount of experimental work, the understanding of this system is converging [11]. Most of the recent work agrees on the following for thermally deposited films at 250–300 K [12–17]: (a) At large thickness (region III), a bcc Fe phase is formed. (b) Below about 4 monolayers (ML) (region I), the ferromagnetic face-centered-tetragonal (fct) Fe phase is obtained. (c) A third phase which consists of antiferromagnetic fcc Fe covered with ferromagnetic fct Fe surface layers can be realized between 5 and 11 ML (region II). It is this rich variety of structural and magnetic phases that makes the Fe/Cu(100) system a unique system in exploring the close correlation between film structure and magnetic properties.

However, several puzzling questions still exist on the ground state magnetic structure in region II: (i) The SDW state has a lower energy than the collinear type-1 AFM state for fcc Fe particles precipitated in a Cu matrix. Should this also be reflected in the ground state magnetic structure of fcc Fe films on Cu(100)? (ii) Theoretically, so far all the *ab initio* calculations on Fe/Cu(100) [18–21] were carried out based on the assumption of collinear spin states. It was not clear whether some noncollinear magnetic structures in regime II were lower in energy than those collinear spin states [21]. (iii) Experimentally a clear oscillatory behavior of the total magnetic moment versus film thickness was observed [11,17], but a quantitative determination of the oscillation is still incomplete, which would be extremely important for establishing a correct theoretical model.

In this Letter, we are going to demonstrate experimentally that except for the top two FM surface layers the SDW state is the magnetic structure of underlying fcc Fe on Cu(100) in region II. As compared to previous work, the uniqueness of our approach to this problem is threefold. (i) *In situ* scanning tunneling microscope (STM) is used together with reflection high energy electron diffraction (RHEED) intensity oscillations and a quartz crystal monitor to measure accurately the deposited film thickness. This is obviously very crucial in determining quantitatively the magnetic moment versus film thickness curve [22]. (ii) Employing the high sensitivity of STM in detecting the phase transition from fcc Fe to bcc Fe [23], it is guaranteed that the magnetic properties to be discussed here are indeed coming from pure fcc Fe instead of a mixed fcc and bcc Fe phase. (iii) Again with the accurate calibration of the absolute film thickness, instead of measuring thickness differences [17], the temperature dependent magnetization ($60 < T < 300$ K) of 6, 7, and 8 ML of Fe on Cu(100) can be measured separately and independently.

The experiment was carried out in a multifunctional ultrahigh vacuum system, equipped with RHEED, STM, low energy electron diffraction (LEED), cylindrical mirror analyzer based Auger electron spectroscopy (AES), and magneto-optical Kerr effect (MOKE). Prior to Fe deposition, the clean Cu(100) surface was prepared by cycles of 1 keV argon-ion bombardment at 300 K until no contaminations were detectable by AES, followed by annealing at

873 K for 15 min. This cleaning procedure was repeated until a sharp (1×1) LEED pattern was observed, coinciding with large atomically flat terraces as seen by STM. The pressure was kept better than 2×10^{-11} mbar during evaporation. The film thickness of Fe on Cu(100) was cross checked by a quartz microbalance, by RHEED oscillations, and by STM with an accuracy within 0.1 ML.

It is noticed that the RHEED oscillations in Refs. [15] and [17] behave quite differently in region I. The first oscillation peak was missing in region I in the former but was clearly seen in the latter. Because of the delicate correlation between the structure and magnetism of this system, the first point to be addressed in the present work is to try to verify that we are all investigating the same system. Figures 1(a) and1(b) show two sets of RHEED oscillations that are obtained under the same film deposition conditions but measured at different azimuthal angles. Based on the fact that we can reproduce both sets of RHEED oscillations reported in Refs. [15] and [17], it is fair to assume that we are dealing with the same system.

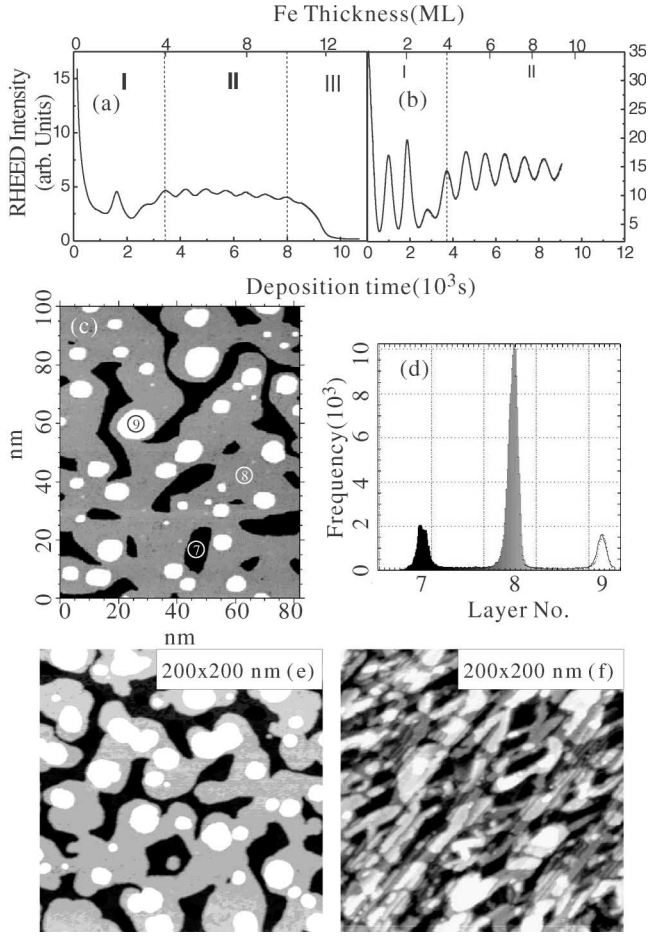

FIG. 1. (a) and (b) Two types of RHEED oscillations for Fe/Cu(100) grown at 300 K; (c) and (d) STM image for 8 ML Fe on Cu(100) and its histogram, 7, 8, and 9 indicate the layer number of Fe; (e) and (f) STM images for 9 ML Fe/Cu(100) before and after cooling.

Controlled by the quartz crystal thickness monitor and RHEED intensity oscillations, the Fe deposition in each experiment is stopped at the desired film thickness. However, the exact final thickness determination is done using STM after film deposition [22]. For example, Fig. 1(c) shows an STM image after deposition of 8 ML Fe on Cu(100), and Fig. 1(d) gives its corresponding histogram, from which it can be seen that the exposed surface area consists of about 80% of the 8th layer, 10% of the 7th layer, and 10% of the 9th layer; i.e., about 90% of the 8th layer is filled, while the missing 10% of this ML goes to the 9th layer. Each film thickness discussed in the following has been determined this way.

It is well known that a martensitic phase transition from fcc Fe to bcc Fe takes place at about 10–12 ML. Because the main focus of this work is on the magnetic structure of fcc Fe in region II, it is very critical to verify that all the magnetic properties to be discussed are really from the fcc Fe phase rather than a mixture of fcc and bcc Fe phases. It has been demonstrated that STM is a very sensitive and powerful technique to detect this martensitic phase transition, since an STM picture with ridges can immediately be observed once the transition from fcc to bcc Fe happens [23]. Based on the accurate thickness calibration, it is determined that the fcc Fe phase becomes unstable at $\sim$9–10 ML. Figures 1(e) and 1(f) are two STM images taken for 9 ML Fe on Cu(100) before and after cooling to 70 K, respectively. It can be seen from Fig. 1(e) that the film as prepared consists of pure fcc Fe, but the phase transition occurs during the heating up to 300 K as shown in Fig. 1(f). Correspondingly, the split spots of the bcc phase are also observed in the LEED pattern when the transition takes place (not shown here). Meanwhile as far as the magnetism is concerned, we realized, by measuring both the polar and longitudinal MOKE loops, that the magnetic moment stays perpendicular to the plane during the cooling while it tends to lie down in the plane irreversibly during the subsequent warming up. After all these careful evaluations it is guaranteed that the magnetism data presented below (taken before warming up) are all from the pure fcc Fe phase.

The polar Kerr rotation angle at remanence as a function of film thickness is measured at 70 K as indicated by the square dots shown in Fig. 2. It can be clearly seen that the oscillation valley is located at $\sim$7 ML, which is an important fact in establishing or verifying any theoretical model. It is also noticed that the MOKE signals at 8.5 and 9 ML do not drop down as would be expected from a collinear type-1 antiferromagnet. Therefore the type-1 antiferromagnetic structure can definitely be excluded for the magnetic structure of fcc Fe on Cu(100) in region II. However, it is impossible in this figure to separate out the contributions from the top two FM surface layers and the uncompensated AFM underlayers. Thus a temperature dependent investigation is further carried out for this purpose.

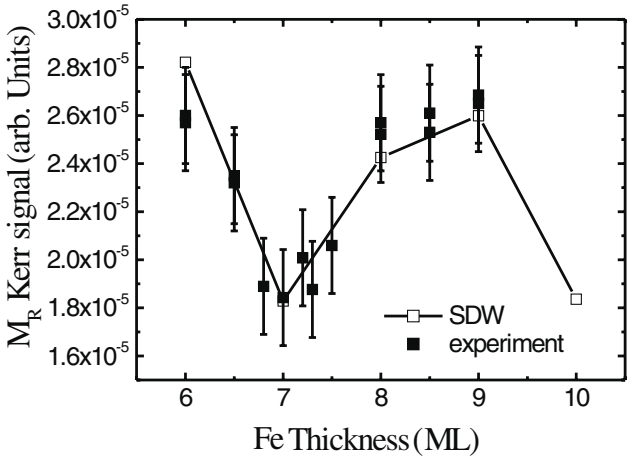

FIG. 2. Polar MOKE as a function of film thickness measured at 70 K together with the fitting curve using incommensurate SDW with $S_z = S_{z0}\cos(qz)$ and $q = 2\pi/2.7d$.

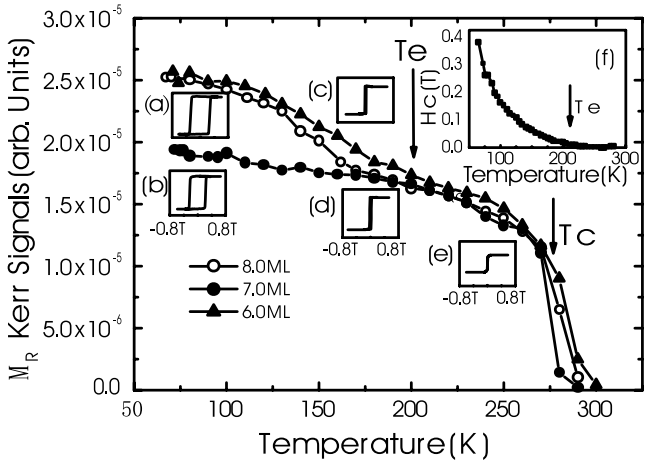

FIG. 3. Temperature dependent magnetization as a function of temperature for 6, 7, and 8 ML Fe on Cu(100), respectively; curves (a)–(e) some representative hysteresis loops at different temperatures; (f) coercivity versus temperature for 8 ML Fe/Cu(100).

Figure 3 shows three representative polar MOKE signal (at remanence) versus temperature curves for 6, 7, and 8 ML of Fe on Cu(100), respectively. Contrary to predictions of the type-1 antiferromagnetic model [10], it is found that the total moment for 7 ML (odd layer) Fe on Cu(100) increases monotonically as the temperature decreases, while the total moment for 6 and 8 ML (even layers) shows an additional steplike increase when the cooling temperature passes ~200 K, the effective ordering temperature Te of the antiferromagnetic underlayers [17]. It is also noticed from this figure [hysteresis curves Figs. 3(a)–3(e)] that the coercivity H_c of these systems increases significantly when the temperature drops below Te. A representative curve of H_c vs T for 8 ML Fe on Cu(100) is plotted in the inset of Fig. 3. Because of its temperature reversibility, the increase of coercivity by 2 orders of magnitude cannot be due to any impurity or defect effects. It is rather a kind of fingerprint of turning on the exchange coupling between the top two FM surface layers and the bulk AFM underlayers below the effective ordering temperature Te. However, no exchange-biased loops are observed under our experimental conditions, presumably due to the fact that the antiferromagnetic pinning effect is not strong enough at this limited number of AFM layers.

Therefore it becomes clear that a type-1 antiferromagnetic structure model does not fit the experimental facts for Fe on Cu(100). By contrast, the SDW model proposed for the magnetic structure of precipitated fcc Fe clusters in a Cu matrix turns out to be a good candidate to explain these new data. A SDW with $S_z = S_{z0}\cos[q(z - z_0)]$ is assumed, where S_z is the z component of magnetic moment, S_{z0} the normalization constant, q the wave vector of SDW, z the position in space along the z direction, and z_0 the initial phase term determined by the choice of axis origin. As far as magnetism is concerned, one can presumably state that the FM/AFM interface is a strongly coupled one as manifested in the inset of Fig. 3(f), while the AFM/Cu interface is a freestanding one because of the fact that Cu is nonmagnetic. It is then deduced from the additional signal increase below Te in Fig. 3 that the Fe magnetic moments at the FM/AFM interface must be ferromagnetically rather than antiferromagnetically coupled to each other. This simply means that $z_0 = 0$, when choosing the origin in the topmost AFM plane (i.e., the third Fe layer from the top). The inset of Fig. 4 shows the incommensurate SDW together with the layer dependent

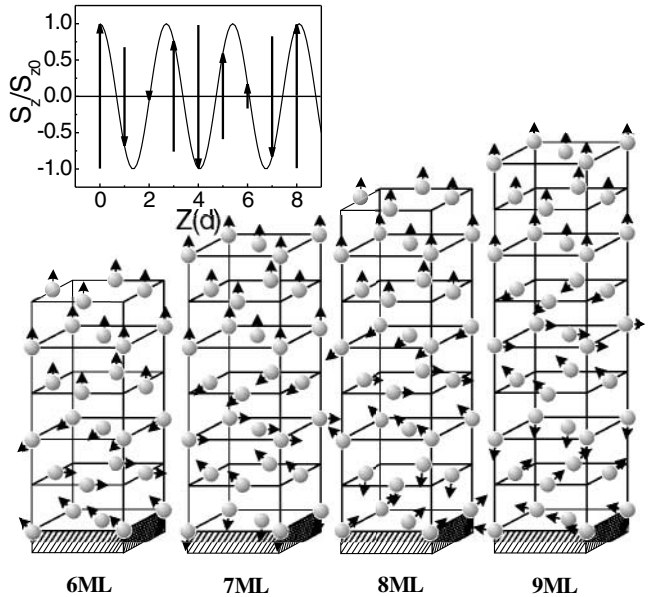

FIG. 4. Magnetic structures proposed for 6, 7, 8, and 9 ML Fe on Cu(100); the inset gives the layer dependent magnetic moments for fcc Fe along the z direction, $z(d) = 0$ corresponding to the first AFM layer. (Note: all the moments drawn here are lying in the planes parallel to the front plane of the structure section.)

magnetic moments along the z direction, for the antiferromagnetic fcc Fe underlayers with a wave vector $q = 2\pi/2.7d$, where d is the interlayer distance of fcc Fe. The wave vector is determined by the curve fitting to Fig. 2 as shown by the solid line. Accordingly the magnetic configurations for 6, 7, 8, and 9 ML Fe on Cu(100) can be constructed one by one as shown in Fig. 4. For example, the magnetic structure of 6 ML Fe on Cu(100) is constructed by aligning the third (counting from the top) Fe layer moment parallel to those of the top two FM surface layers, then the moments of the three lower antiferromagnetic fcc Fe layers are set according to the local value of their z component in the inset. It is obvious from the inset that the contributions to the total film moment from the second $[z(d) = 1]$ and the fourth $[z(d) = 3]$ AFM layers almost cancel each other. The third AFM layer $[z(d) = 2]$ contributes only a little to the total signal signal, leading to a situation that only the first AFM layer $[z(d) = 0]$ of the total four AFM fcc Fe underlayers contributes effectively to the total magnetization. It is this uncompensated AFM part that causes the additional increase of magnetization below Te in Fig. 3. A similar analysis using the inset of Fig. 4 yields immediately that the moments of five AFM fcc Fe underlayers almost cancel each other completely, which exactly explains why the valley in Fig. 2 is located at 7 ML Fe on Cu(100), and why the 7 ML film magnetization in Fig. 3 increases only weakly even when the temperature drops below Te. The results for 8 and 9 ML can equally well be understood this way.

Finally several points are worth mentioning. (1) According to the amount of Kerr rotation angle increase below Te in Fig. 3, the magnetic moment per Fe atom in the incommensurate SDW fcc Fe is estimated to be about the same as that of the top two FM fct Fe surface layers. (2) In principle, a spiral-spin-density wave for the fcc Fe underlayers cannot be excluded, because the information obtained in this experiment is limited only along the z direction, while the layer dependent in-plane magnetic structure is still an open question.

D. Qian and X. F. Jin acknowledge the support from MPI Halle during their stay in Halle. X. F. Jin also acknowledges the partial supports from the National Natural Science Foundation of China, the Cheung Kong Scholars Program, Hong Kong Quishi Science Foundation, and Y. D. Fok Education Foundation.

*Corresponding author.
Email address: xfjin@fudan.ac.cn

[1] C. S. Wang, B. M. Klein, and H. Krakauer, Phys. Rev. Lett. **54**, 1852 (1985).
[2] F. J. Pinski, J. Staunton, B. L. Gyorffy, D. D. Johnson, and G. M. Stocks, Phys. Rev. Lett. **56**, 2096 (1986).
[3] V. L. Moruzzi, P. M. Marcus, K. Schwarz, and P. Mohn, Phys. Rev. B **34**, 1784 (1986).
[4] O. N. Myrasov, V. A. Gubanov, and A. I. Liechtenstein, Phys. Rev. B **45**, 12 330 (1992).
[5] M. Uhl, L. M. Sandratskii, and J. Kubler, Phys. Rev. B **50**, 291 (1994).
[6] M. Körling and J. Ergon, Phys. Rev. B **54**, R8293 (1996).
[7] Y. M. Zhou, D. S. Wang, and Y. Kawazoe, Phys. Rev. B **59**, 8387 (1999).
[8] Y. Tsunoda, J. Phys. C **1**, 10 427 (1989).
[9] Y. Tsunoda, Y. Nishioka, and R. M. Nicklow, J. Magn. Magn. Mater. **128**, 133 (1993).
[10] R. E. Camley and D. Q. Li, Phys. Rev. Lett. **84**, 4709 (2000).
[11] A. Berger, B. Feldmann, H. Zillgen, and M. Wuttig, J. Magn. Magn. Mater. **183**, 35 (1998).
[12] K. Kalki, D. D. Chambliss, K. E. Johnson, R. J. Wilson, and S. Chiang, Phys. Rev. B **48**, 18 344 (1993).
[13] M. Wuttig, B. Feldmann, J. Thomassen, F. May, H. Zillgen, A. Brodde, H. Hannemann, and H. Neddermeyer, Surf. Sci. **291**, 14 (1993).
[14] H. Zillgen, B. Feldmann, and M. Wuttig, Surf. Sci. **321**, 32 (1994).
[15] J. Thomassen, B. Feldmann, M. Wuttig, and H. Ibach, Phys. Rev. Lett. **69**, 3831 (1992).
[16] W. Keune, T. Ezawa, W. A. A. Macedo, U. Glos, K. P. Schletz, and U. Kirschbaum, Physica (Amsterdam) **161B**, 269 (1989).
[17] D. Li, M. Freitag, J. Pearson, Z. Q. Qiu, and S. D. Bader, J. Appl. Phys. **76**, 6425 (1994); Phys. Rev. Lett. **72**, 3112 (1994).
[18] C. L. Fu and A. J. Freeman, Phys. Rev. B **35**, 925 (1987).
[19] G. W. Fernando and B. R. Cooper, Phys. Rev. B **38**, 3016 (1988).
[20] T. Kraft, P. M. Marcus, and M. Scheffler, Phys. Rev. B **49**, 11 511 (1994).
[21] T. Asada and S. Blügel, Phys. Rev. Lett. **79**, 507 (1997).
[22] X. F. Jin, J. Barthel, J. Shen, S. S. Manoharan, and J. Kirschner, Phys. Rev. B **60**, 11 809 (1999).
[23] J. Shen, C. Schmidthals, J. Woltersdorf, and J. Kirschner, Surf. Sci. **407**, 90 (1998).